Simulations of XV-15 Rotor Flows in Hover Using OVERFLOW

Seokkwan Yoon*, Thomas H. Pulliam*, and Neal M. Chaderjian*
NASA Ames Research Center, Moffett Field, California 94035

Unsteady turbulent flow simulations were performed to investigate the effect of turbulence models on the prediction of rotorcraft hover efficiency (figure of merit). One and two-equation eddy viscosity models were studied, including the use of zonal approximations and detached eddy simulation. Skin friction coefficients were compared with available experimental data. The effects of grid resolution, distance to the far-field boundary, and solution convergence were investigated. Coarse grids, close proximity of far-field boundaries, and inadequate convergence were found to artificially increase the predicted figure of merit from its asymptotic value.

I. Introduction

Despite rapid advances in Computational Fluid Dynamics (CFD) during the past several decades, accurate simulation of rotorcraft flows is still challenging due to the inherent complexity of vortex wakes. Unlike fixed-wing aircraft, a rotor blade can encounter its own tip vortex and the tip vortices of other blades. As a result, blade vortex interaction (BVI) can have a significant effect on the performance of the vehicle. One common result of BVI is sharp azimuthal peaks in the sectional coefficients for a rotor in forward flight, often generating significant noise. However, the close proximity of a vortex to a rotor blade in hover can also influence a blade's boundary layer and greatly affect a turbulence model's ability to accurately predict the figure of merit (FM).[1]

One of the primary goals of the analysis of rotors in hover is to predict the forces generated and power required by the rotating blades so that the most efficient rotor can be designed. The FM is a measure of rotor hovering efficiency, defined as the ratio of ideal power required to hover (from actuator disk theory) to the actual power required to hover. Thus, the FM compares the actual rotor performance with the performance of an ideal rotor, which only includes the induced power.[2]

The OVERFLOW[3,4] Reynolds-averaged Navier-Stokes (RANS) code was used successfully to simulate the flow fields of the V-22 Osprey and UH-60A isolated rotors in hover and forward flight.[1,5-9] This time-dependent CFD code utilizes overset grids to model complex rotorcraft geometries. The use of near-body (NB) and off-body (OB) overset grids also allows for the use of different turbulence model options in different grid zones. The objective of the present paper is to investigate the effects of various zonal turbulence modeling approaches on the FM and skin friction coefficient for an isolated rotor in hover, especially with the Spalart-Allmaras (SA) one-equation model.[10-12] The Shear Stress Transport (SST) two-equation model[13] is also considered. Moreover, the effect of far-field boundary proximity to the rotor is examined, and the computed results are compared with XV-15 wind-tunnel data.[14] The following sections discuss the numerical approach, different zonal turbulence modeling options used in this study, CFD results, and concluding remarks.

II. Numerical Approach

OVERFLOW solves the RANS equations on structured overset grids. The current time-accurate approach consists of an inertial coordinate system where NB curvilinear O-grids (rotor blades and hub) rotate through a fixed

* Fundamental Modeling and Simulation Branch, NASA Advanced Supercomputing Division.

Presented at the Fifth Decennial AHS Aeromechanics Specialists' Conference; San Francisco, CA; January 22-24, 2014.

OB Cartesian grid system. The medium-sized XV-15 isolated rotor grid system used in this study is shown in Fig. 1. A uniformly spaced OB Cartesian grid surrounds the rotor blades and hub and resolves the rotor wake region of interest. Coarser "brick-grids" efficiently expand the grid system to the far field, where each successive brick grid is twice as coarse as its previous neighbor. The XV-15 isolated rotor consists of three highly twisted rotor blades and a simplified hub. Each rotor blade consists of three O-grids, one for the main rotor blade and two "cap-grids" for the inboard and outboard tips. The grid spacing normal to solid surfaces maintains $y^+<1$. Different grid resolutions are used in this study and summarized in Table 1. Note that the resolved wake region for the three grid resolutions have uniform grid spacing ranging from 5% c_{tip} to 20% c_{tip}. Care is taken to make sure the NB grid spacing is similar to the OB grid spacing where the grids overlap. Both the NB and OB grids are therefore refined together, where the NB grid spacing is approximately twice as fine in each wall-parallel direction as the previous coarser grid.

Grid Name	Number of Grids	NB Grid Points (Million)	OB Grid Points (Million)	Total (Million)	OB Resolution (Percent c_{tip})
Coarse	42	5.4	4.3	9.7	20%
Medium	62	18.6	28.6	47.2	10%
Fine	124	79.8	207.1	286.9	5%

Table 1. Overflow overset grid system for the XV-15 isolated rotor and simplified hub.

OVERFLOW solves the Navier-Stokes equations using finite differences with a variety of numerical algorithms and turbulence models.[3] Up to 6th-order spatial accuracy for inviscid fluxes and 2nd-order time accuracy are available.[4] In this study, the Pulliam-Chaussee[15] diagonal central difference algorithm is used with the 5th-order spatial differencing option.[4] Dual time-stepping is used to advance the simulation in time with 2nd-order time accuracy. The physical time step corresponds to 0.25 degrees rotor rotation, together with 15 dual-time sub-iterations. This typically provides for a 1.75 sub-iteration residual drop. This numerical approach and time step was previously validated for similar isolated rotor flows.[1,7,8]

III. Turbulence Modeling

Direct Numerical Simulation (DNS) solves the time-dependent Navier-Stokes equations by resolving a wide range of spatial and temporal scales of turbulence. Since DNS requires a large number of grid points to resolve the Kolmogorov dissipative scales, simulating high Reynolds number flow is not feasible even with today's most powerful supercomputers. Large Eddy Simulation (LES) requires less computational resources than DNS by modeling the smallest turbulent length scales using a sub-grid model while still grid resolving the large eddies. However, the grid requirements for high Reynolds number LES calculations are still impractical. Since the high cost of computation for pure LES comes from the near-wall region, hybrid models like detached eddy simulation[10] (DES) have been developed. The DES approach alleviates the difficulty of resolving the smallest scales by using a RANS turbulence model in the boundary layer and LES to grid-resolve the largest scales outside the boundary layer. The RANS turbulence model becomes the LES sub-grid model in the region outside the boundary layer.

While RANS methods produce mostly inaccurate solutions for high-speed flows with large separation regions, the DES approach of Spalart[10] in conjunction with the one-equation Spalart-Allmaras[11] model has predicted[1,7-8] unsteady flows with improved accuracy by resolving the dynamics of the dominant larger turbulent length scales.

The SA-RANS model, implemented for the present study, uses the Boussinesq approximation to relate the Reynolds stresses to a kinematic turbulent eddy viscosity and the mean strain-rate tensor. The turbulent eddy viscosity is given by the expression

$$\nu_t = \tilde{\nu} f_{v1} \tag{1}$$

The turbulence transport equation for the turbulence variable $\tilde{\nu}$, is given by

$$\frac{D\tilde{\nu}}{Dt} = P(\tilde{\nu}) - D(\tilde{\nu}) + \mathcal{D}(\tilde{\nu}) \tag{2}$$

where D/Dt is the material time derivative. The right-hand side consists of turbulence production, dissipation and diffusion source terms. The production is given by

$$P(\tilde{\nu}) = C_{b1}\tilde{\nu}\left(\Omega + \frac{\tilde{\nu}}{\kappa^2 d^2} f_{v2}\right) \tag{3}$$

the dissipation by

$$D(\tilde{\nu}) = C_{w1} f_w \left(\frac{\tilde{\nu}}{d} \right)^2 \tag{4}$$

and the diffusion by

$$\mathcal{D}(\tilde{\nu}) = \frac{1}{\sigma} \left[\nabla \cdot \left((\nu + \tilde{\nu}) \nabla \tilde{\nu} \right) + C_{b2} (\nabla \tilde{\nu})^2 \right] \tag{5}$$

The constants C_{b1}, C_{b2}, C_{w1}, κ, σ, and functions f_{v1}, f_{v2}, f_w, are described by Spalart and Allmaras.[11] The damping function, f_{v1}, reduces ν_t near a solid wall. Note that the OVERFLOW CFD code uses the magnitude of vorticity, Ω, in place of the strain-rate, since these two are approximately equal in a boundary layer and the vorticity is readily available in the OVERFLOW code. The turbulence length scale, d, is defined as the distance to the nearest wall. The accuracy of the SA-RANS model depends strongly on the source terms in Eq. (2), which were primarily developed for attached boundary-layer flows along flat plates, wings, fuselages, etc.

Chaderjian and Buning[1] showed that the turbulence length scale, d, plays a key role in accurately determining the rotor FM. A problem occurs deep within the rotor wake, where d may be several rotor radii in length. In this case, d no longer represents an estimate of the largest turbulent eddy in the local flow, but rather, a very large geometric parameter. Note that when d is very large the turbulence dissipation, Eq. (4), becomes very small. On the other hand, the strong tip vortices in the lower wake can generate significant turbulence production from Eq. (3). Over time, this imbalance in turbulence production and dissipation in the lower wake can result in excessively large eddy viscosities. These large viscosities can migrate up the vortex wake after several rotor revolutions, and under BVI conditions, infiltrate the blade boundary layers. When this happens, the rotor blade drag and torque increase significantly and artificially, resulting in large FM errors and an under-prediction of rotor efficiency.

The DES model is a RANS/LES hybrid approach that mitigates the problem of artificially large eddy viscosity. The turbulence length scale used in Eqns. 1-5 is modified by Eq. (6) by taking the minimum of the distance from the wall, d, and the local grid spacing, $\Delta=\max(\Delta x, \Delta y, \Delta z)$. The fixed coefficient is given by $C_{DES}=0.65$.

$$\bar{d} = \min\left(d, C_{DES}\Delta\right) \tag{6}$$

This simple but crucial change can be viewed in two different ways. From a numerical perspective the length scale in Eq. (6) has been significantly reduced which allows the turbulence dissipation in Eq. (4) to remain active in the vortex wake below the rotor plane. This prevents the turbulent eddy viscosity from growing to unrealistic values. The torque therefore remains unaffected, compared to the process described above, and the FM is accurately predicted. A physical interpretation views the modified length scale as an implicit filter, where the largest turbulent eddies are now grid-resolved on the order of size Δ. All smaller eddies are modeled by a reduced turbulent eddy viscosity. This DES approach provides a rational way to reduce the length scale, and hence the turbulent eddy viscosity, based on a physical model.

The DES approach assumes that the wall-parallel grid spacing, Δ, exceeds the thickness of the boundary layer so that the RANS model remains active near solid surfaces. If $\Delta<\delta$, the boundary layer thickness, then the DES Reynolds stresses can become under-resolved within the boundary layer and may lead to non-physical results, including grid-induced separation. Using delayed detached eddy simulation[12] (DDES), the RANS mode is prolonged and is fully active within the boundary layer. The wall-parallel grid spacing used in this study does not violate the hybrid-LES validity condition. Thus DES and DDES should give similar results.

Another engineering approach is to simply zero out the right-hand side of Eq. (2) in the vortex wake, below the rotating blades. This zonal approach allows the turbulent eddy viscosity that is generated in the NB rotor-blade grids to convect downward unchanged along a streamline into the lower-wake OB grids. In this way, the turbulent eddy viscosity is controlled and never allowed to grow to very large values, which can artificially reduce the FM. This approach is referred to as the Laminar Off Body (LOB) approach in OVERFLOW because it does not account for turbulence production, dissipation or diffusion in the lower wake OB grids. As the grid is refined, the DES approach is consistent with LES, whereas the LOB engineering approach is not.

Menter's two-equation turbulence model, also known as the Shear Stress Transport (SST)[13] model, is another RANS model examined in this study. The SST turbulence model blends the k-omega model for the inner boundary layer with the k-epsilon model for the outer boundary layer. Furthermore, the redefined SST eddy viscosity accounts for the effect of transport of turbulent shear stress. The SST model has been used for many external flows with adverse pressure gradients.

IV. Results

Three-dimensional unsteady fully turbulent flow simulations were performed using OVERFLOW. Three levels of grid resolution were evaluated. The number of grid points for coarse, medium, and fine grids were approximately 10 million, 47 million, and 287 million, respectively. Grid resolution details are summarized in Table 1. Most results were produced on the medium grid using 1024 cores on the Pleiades system, a supercomputer that currently has 162,496 cores (166 racks) and a total of 417 TB memory at the NASA Advanced Supercomputing Division. The speed of each processor of Intel Xeon Ivy Bridge node is 2.8 GHz, and the available memory is 64 GB per node. A typical fine-grid job requires approximately 240 hours of wall-clock time for 30 rotor revolutions. Since the size of the time step is 0.25 deg, 1440 steps are needed for a single revolution.

The test problem investigated here is a θ=10 deg collective (pitch) case[14] for an isolated XV-15 rotor in hover. This is a BVI case from the point of view that the rotor vortices are sufficiently close to the rotor blades so that they significantly affect the blade boundary layers and rotor FM. The local tip Mach number is 0.69 and the Reynolds number based on the tip chord is 4.9 million. Figure 2 provides a visualization of the overall medium grid rotor wake structure, including a top view of the rotor blade tip vortices using iso-surfaces of the Q-criterion, and a side view of vorticity contours on a cutting plane colored by vorticity magnitude.

First, a grid refinement study was carried out using RANS in the NB grids and LOB in the OB grids. While this approach[5,6] allows the turbulent eddy viscosity to freely convect between the NB grids and the OB grids, vortex diffusion and the eddy viscosity are controlled by turning off all turbulence production, dissipation, and diffusion source terms (Eq. 2) in the OB vortical regions. The SA one-equation model was used as the base turbulence model. Figure 3 shows a comparison of FM histories for the coarse, medium, and fine grids. The FM represents a running mean with a period of one rotor revolution. Contrary to a common practice of using ten or so revolutions to obtain a solution, 20-30 revolutions may be required for the FM to fully converge, i.e., the variation is relatively flat. Table 2 summarizes the computed and measured FM. The difference between the medium and fine grid FM is small, and they compare best with experiment. Note that the coarse grid FM is artificially high and has the largest error. This trend tends to be the case in practice.[1] Thus, using too coarse of a grid may give an artificially elevated FM.

Case	FM	Difference from Experiment
Coarse Grid	0.778	2.4%
Medium Grid	0.772	1.6%
Fine Grid	0.770	1.3%
Experiment[14]	0.760	–

Table 2. Figure of Merit. M_{tip}=0.69, Re_{Ctip}=4.9 million, θ=10°.

Figures 4a-4f show computed skin friction coefficients (C_f) compared with the available experimental data[14] at the 17, 28, 50, 72, 83 and 94 percent radial stations. The C_f was measured using an oil-film interferometric technique.[14] The differences between the medium and fine grid results are small for each rotor-blade radial station. The coarse grid C_f differs most from the medium and fine grid results at the most inboard station, r/R=0.17. The computed C_f capture the experimental trends for all radial stations, and compare especially well at the outboard radial stations (Figs. 4c-f) for $x/c > 0.2$. Most radial stations show the computed C_f over-predict the experimental values near the blade leading edge, i.e., when $x/c < 0.2$. The leading edge and inboard station discrepancies indicate that a turbulent transition model is probably warranted to fully capture the C_f. Fortunately, the prediction of FM seems to be relatively insensitive to the C_f. These results indicate the medium grid resolution appears to be sufficient to accurately capture the FM and C_f.

Most modern CFD codes, including OVERFLOW, use far-field boundary conditions based on the method of characteristics. However, since the characteristic boundary conditions are often based on one-dimensional theory, far-field boundaries that are located too close to a body can create spurious reflections of acoustic waves in three-dimensional problems and affect the final results. The problem is more complicated in rotorcraft simulation because the flows are inherently unsteady with several blade-tip vortices, and it takes a long time to establish the low-speed induced flow for hover. Figure 5 shows how the converged FM varies with proximity of the far-field boundary location. Note that as the far-field boundary is brought closer to the rotor, the FM rises significantly. The FM approaches its asymptotic value when the far-field boundary is located about 15-20R from the rotor.

Figure 6 shows computed surface-flow streamlines (relative to the rotating blade) for the XV-15 in hover. This flow visualization reveals a complex three-dimensional separation line along the inboard part of the blade, where the surface flow is directed more along the radial direction than the streamwise direction. The experimental C_f suggests that the present BVI case is mostly turbulent at the outboard stations, but significant laminar to turbulent transition

occurs at the mid-inboard stations, i.e., r/R=17-28%. These transitional affects were not predicted because the CFD simulation was treated as fully turbulent.

To investigate the effect of zonal turbulence modeling, the LOB, DES, and DDES OB models in conjunction with the RANS NB model are compared with the experimental data[14] at the 94% radial station. Each of these cases uses the SA turbulence model. Figure 7 shows that there is little difference in predicted C_f between the OB models. Next, RANS, DES, and DDES are employed as the NB model in conjunction with the LOB OB model. In Fig. 8, moderate differences in C_f are observed between various NB models on the medium grid. NB turbulence models understandably affect the C_f more than OB models, especially when reduced eddy-viscosity models are used in the OB grids. The differences, however, seem to reduce considerably on the fine grid as shown in Fig. 9. So the finest mesh is less sensitive to the choice of the NB option, i.e., fully RANS or DES.

Results from the SST model are now compared to those from the SA model. Here, both models use DDES for both NB and OB grids. Figure 10 shows that the FM using SST-DDES is somewhat lower than the SA-DDES result. The FM values are summarized and compared with experiment in Table 3. The SST FM is slightly closer to experiment that the SA FM. The SST separation line is slightly ahead of the SA model, and may account for the lower predicted FM. Figure 11 shows a top view of SA and SST surface streamlines for the entire rotor blade. The k-omega based models are known to be susceptible to separation at low Reynolds numbers, so the lower FM may be fortuitous. An oblique view of surface streamlines with pressure contours near the outboard rotor-blade tip is shown in Fig. 12. There is minimal difference between surface flow patterns and the pressure field near the rotor-blade tip.

Turbulence Model (Fully DDES)	FM	Difference from Experiment
Spalart-Allmaras (SA)	0.772	1.6%
Shear Stress Transport (SST)	0.767	0.9%
Experiment[14]	0.760	–

Table 3. Effect of turbulence model on FM. M_{tip}=0.69, Re_{Ctip}=4.9 million, θ=10°.

Conclusions

Accurate prediction of the FM for an isolated XV-15 rotor depends not only on the choice of turbulence models but also on the grid resolution. A grid refinement study shows that coarse grids tend to produce an erroneously higher FM. Contrary to a common CFD practice of running ten or so revolutions to obtain solutions, 20-30 revolutions are often required for the XV-15 FM to fully converge. Also, the distance from the rotor to the far-field boundary has a significant effect on the FM. The asymptotic FM is reached when the far-field boundary is located about 15-20 rotor radii away from the rotor. A comparison of predicted C_f with the experimental measurements shows that near-body turbulence models affect the accuracy of solutions more than off-body models as long as reduced eddy-viscosity models are used for the off-body grids. Flow visualization reveals a complex three-dimensional separation along the inboard part of the rotor blade, where surface flow patterns are more in the radial direction than the streamwise direction. The experimental C_f data suggest the boundary layers are turbulent when x/c>20%. Moreover, the mid-span experimental C_f values indicate laminar-turbulent transition. The present computations do not include transitional models. Nevertheless, the present fully-turbulent flow computations show relatively good C_f agreement with experiment over most of the rotor blade. The SST two-equation model predicts a lower FM, which is closer to experiment than the SA one-equation model. However, the k-omega based SST model is known to be susceptible to flow separation, which can lower the FM.

Acknowledgments

The authors would like to thank Mr. Henry Lee and Dr. Jasim Ahmad of NASA Ames Research Center for providing the CFD grids and software to compute the skin-friction coefficients.

References

[1]Chaderjian, N. M. and Buning, P., "High Resolution Navier-Stokes Simulation of Rotor Wakes," AHS 67th Annual Forum, May 2011.

[2]Johnson, W., *Helicopter Theory*, Dover Publications, 1994.

[3]Nichols, R., Tramel, R., and Buning, P., "Solver and Turbulence Model Upgrades to OVERFLOW2 for Unsteady and High-Speed Flow Applications," AIAA Paper 2006-2824, June 2006.

[4]Pulliam, T. H., "High Order Accurate Finite-Difference Methods: as seen in OVERFLOW," AIAA Paper 2011-3851, June 2011.

[5]Holst, T. L. and Pulliam, T. H., "Overset Solution Adaptive Grid Approach Applied to Hovering Rotorcraft Flows," AIAA Paper 2009-3519, June 2009.
[6]Potsdam, M. and Pulliam, T. H., "Turbulence Modeling Treatment for Rotorcraft Wakes," AHS Aeromechanics Specialists Meeting, Jan. 2008.
[7]Chaderjian, N. M. and Ahmad, J. U., "Detached Eddy Simulation of the UH-60 Rotor Wake using Adaptive Mesh Refinement," AHS 68th Annual Forum, May 2012.
[8]Ahmad, J. U. and Chaderjian, N. M., "High-Order Accurate CFD/CSD Simulation of the UH60 Rotor in Forward Flight," AIAA Paper 2011-3185, June 2011.
[9]Kaul, U. K. and Ahmad, J. U., "Skin Friction Predictions over a Hovering Tilt-Rotor Blade Using OVERFLOW2," AIAA Paper 2011-3186, June 2011.
[10]Spalart, P. R., W-H. Jou, Strelets, M., and Allmaras, S. R., "Comments on the Feasibility of LES for Wings and on a Hybrid RANS/LES Approach," *Advances in DNS/LES,* Greyden Press, 1997, pp. 137-147.
[11]Spalart, P. R. and Allmaras, S. R., "A One-Equation Turbulence Model for Aerodynamic Flows," AIAA Paper 1992-0439, Jan. 1992.
[12]Spalart, P. R., "Detached-Eddy Simulation," *Annual Review of Fluid Mechanics*, Vol. 41, 2009, pp. 181-202.
[13]Menter, F. R., "Two-Equation Eddy-Viscosity Turbulence Models for Engineering Applications," *AIAA Journal*, Vol. 32, Aug. 1994, pp. 1598-1605.
[14]Wadcock, A.J., Yamauchi, G.K., and Driver, D.M., "Skin Friction Measurements on a Hovering Full-Scale Tilt Rotor" *Journal of the American Helicopter Society*, Vol. 44, No. 4, Oct. 1999, pp. 312-319.
[15]Pulliam, T. H., and Chaussee, D. S., "A Diagonal Form of an Implicit Approximate-Factorization Algorithm," *Journal of Computational Physics*, Vol. 39, No. 2, 1981, pp. 347-363.

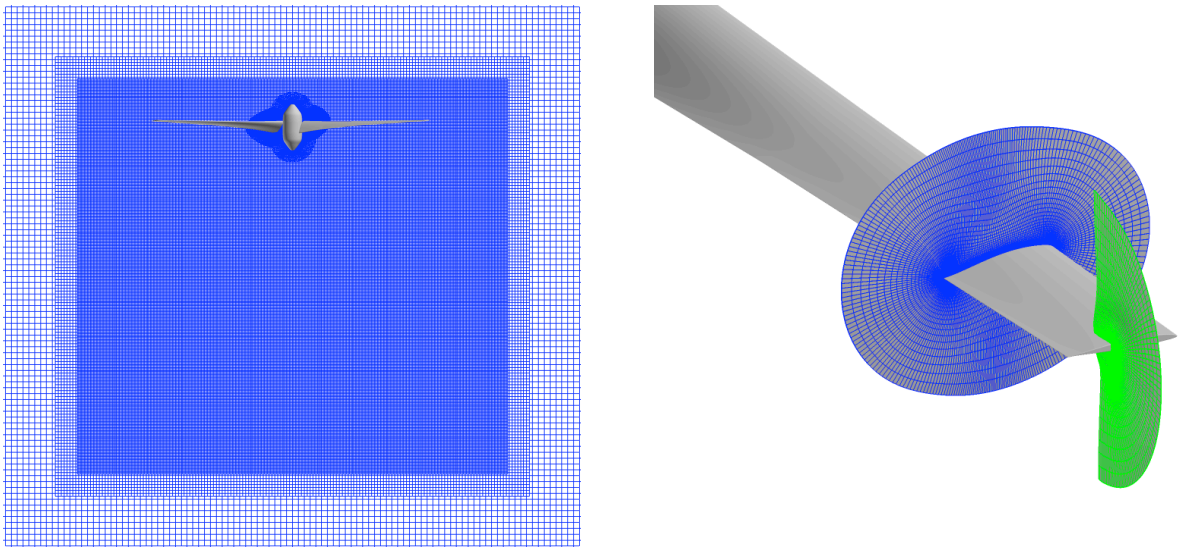

a) Fixed OB Cartesian grids. b) Rotating NB curvilinear rotor-blade grids.

Figure 1. Overflow medium overset grid system for an isolated XV-15 rotor and simplified hub in hover.

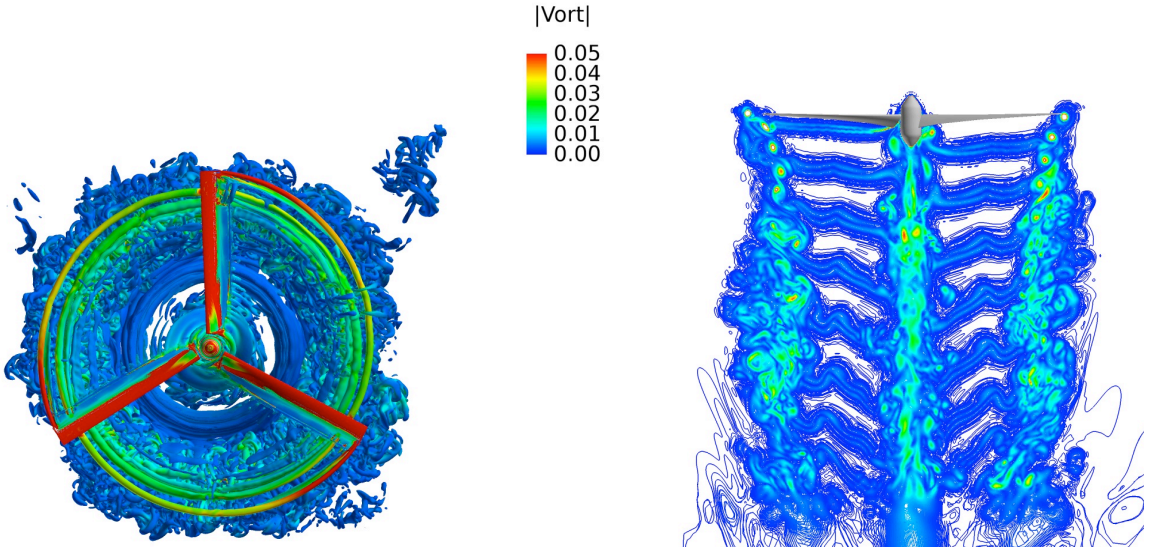

a) Top view of vortex wake, q-criterion.

b) Side view of vorticity contours on a cutting plane.

Figure 2. Flow visualization of XV-15 rotor in hover. M_{tip}=0.69, Re_{Ctip}=4.9 million, θ=10°, SA-RANS/SA-LOB.

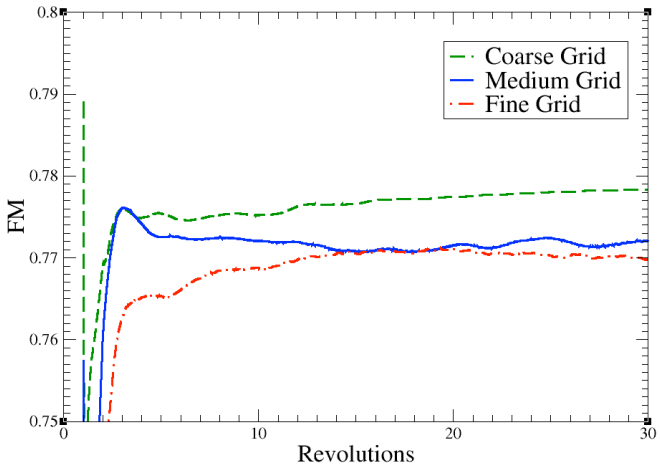

Figure 3. Grid refinement effects on FM. M_{tip}=0.69, Re_{Ctip}=4.9 million, θ=10°, SA-RANS/SA-LOB.

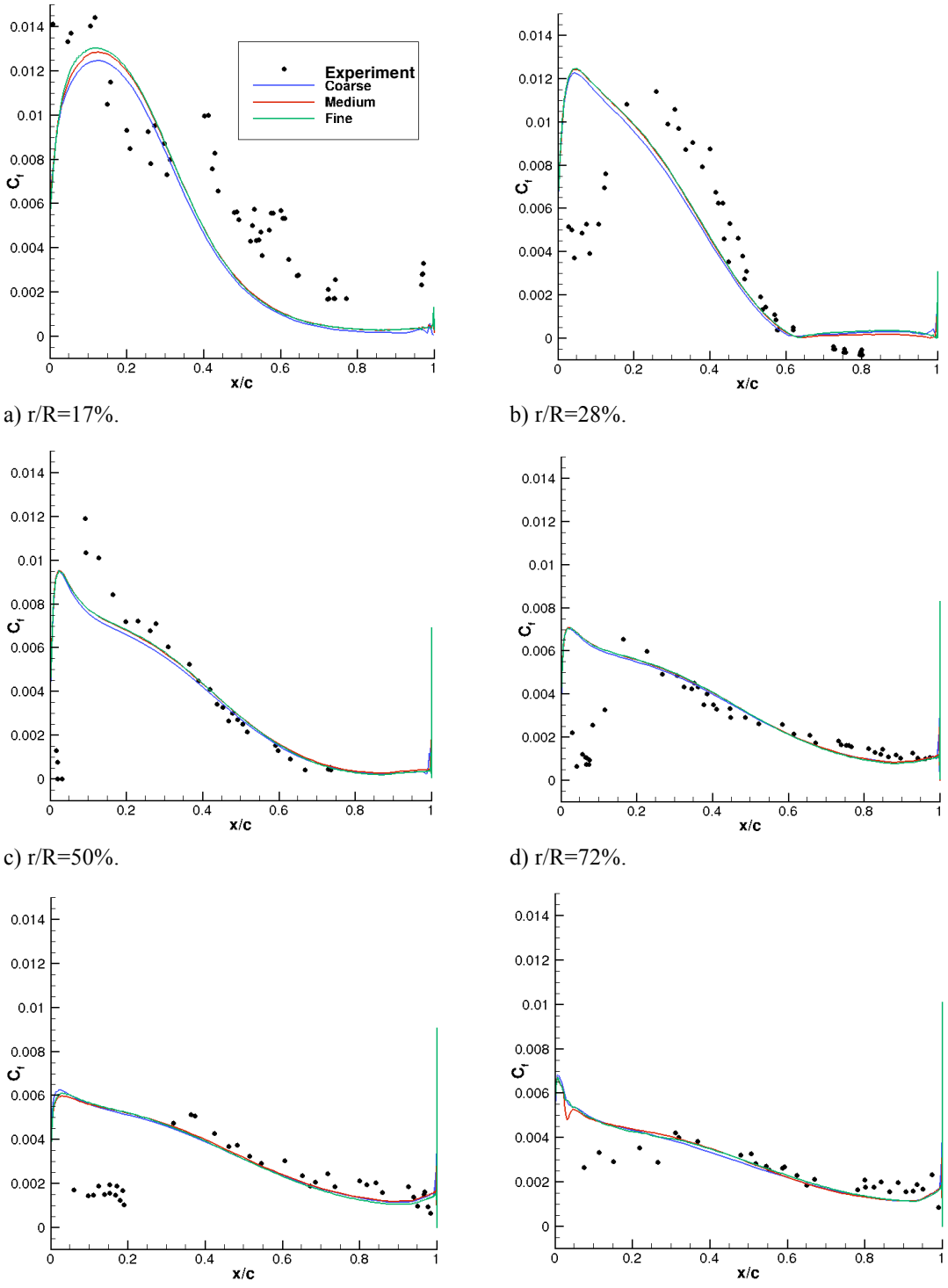

a) r/R=17%.

b) r/R=28%.

c) r/R=50%.

d) r/R=72%.

e) r/R=83%.

f) r/R=94%.

Figure 4. Skin friction coefficient at selected radial stations. M_{tip}=0.69, Re_{Ctip}=4.9 million, θ=10°, SA-RANS/SA-LOB.

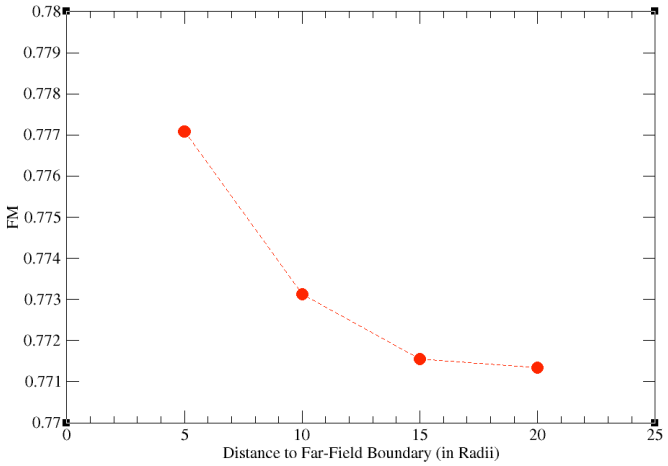

Figure 5. Effect of distance from the rotor to the far-field boundary on the medium grid FM. M_{tip}=0.69, Re_{Ctip}=4.9 million, θ=10°, SA-RANS/SA-LOB.

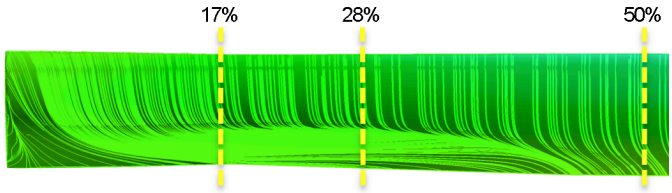

Figure 6. Surface-flow streamlines on the inboard portion of the rotor blade. Dashed lines are experimental radial stations. M_{tip}=0.69, Re_{Ctip}=4.9 million, θ=10°, SA-RANS/SA-LOB.

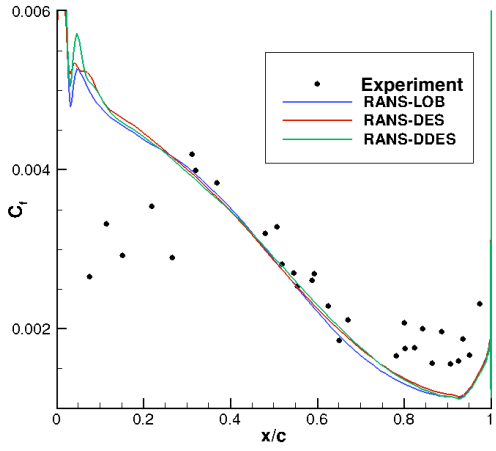

Figure 7. Medium grid comparison of different OB SA turbulence model approaches with the same NB SA-RANS turbulence model, r/R=94%.

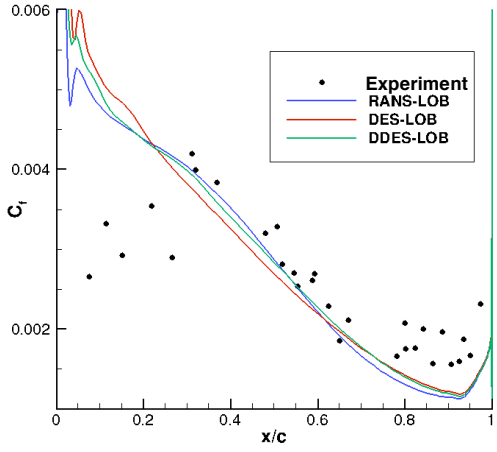

Figure 8. Medium grid comparison of different NB SA turbulence model approaches with the same OB SA-LOB turbulence model, r/R=94%.

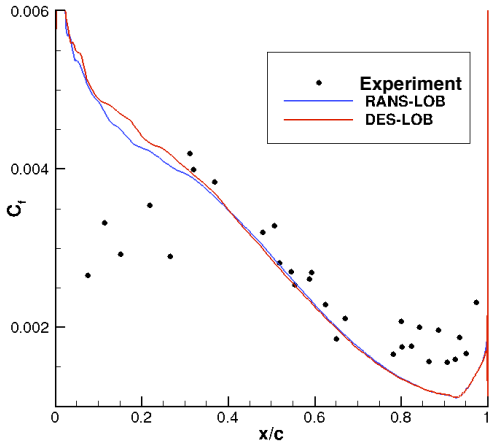

Figure 9. Fine grid comparison of different NB SA turbulence models with the same OB SA-LOB turbulence model, r/R=94%.

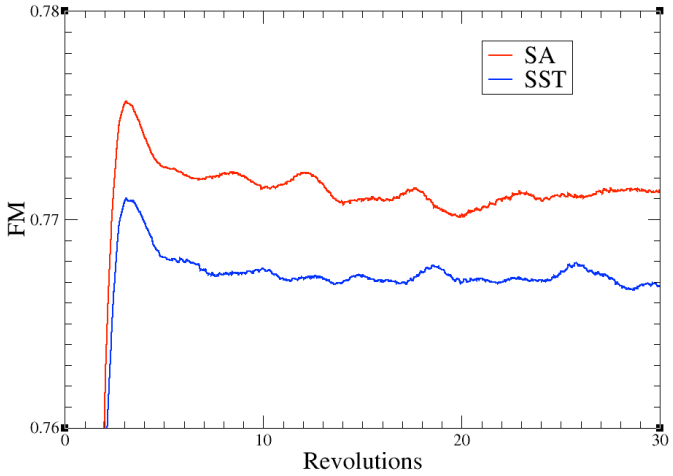

Figure 10. Comparison of FM time histories for the SA and SST turbulence models. M_{tip}=0.69, Re_{Ctip}=4.9 million, θ=10°. DDES is used for both NB and OB grids.

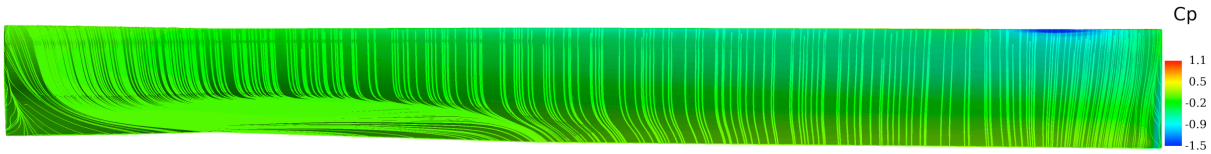

a) SA turbulence model.

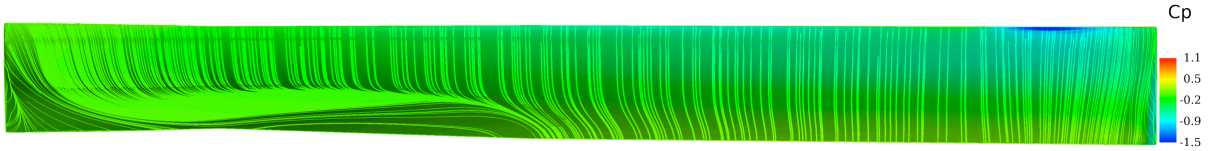

b) SST turbulence model.

Figure 11. Comparison of the upper rotor blade surface-flow streamlines using the SA and SST turbulence models. M_{tip}=0.69, Re_{Ctip}=4.9 million, θ=10°. Both turbulence models use DDES on the NB and OB grids.

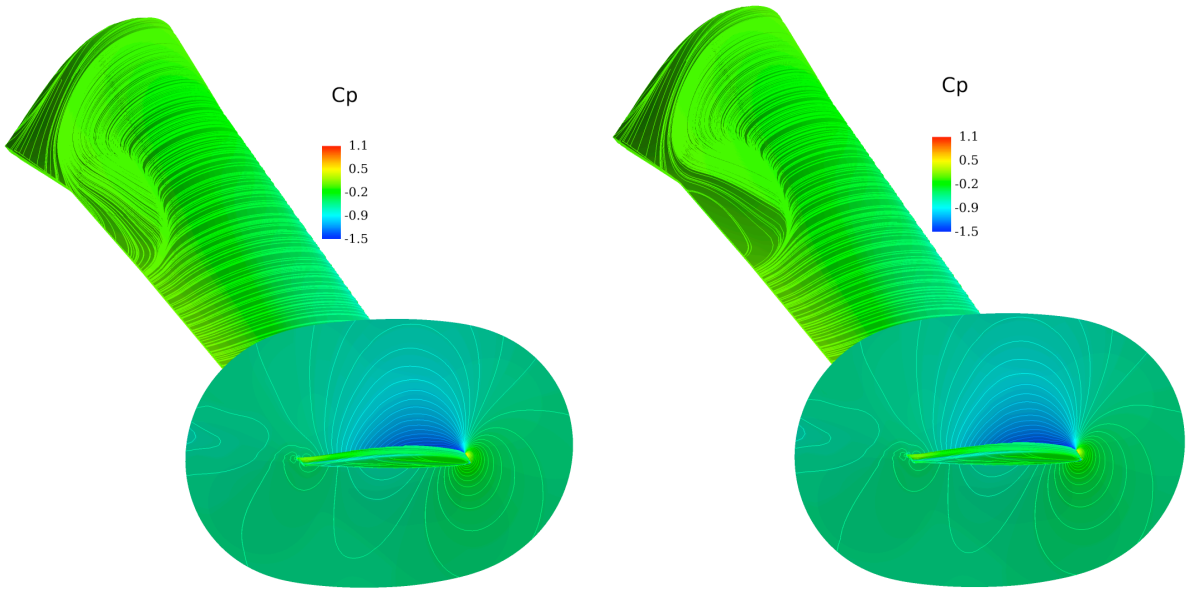

a) SA turbulence model.

b) SST turbulence model.

Figure 12. Comparison of upper rotor blade surface-flow streamlines and the pressure coefficient field near the blade tip using the SA and SST turbulence models. M_{tip}=0.69, Re_{Ctip}=4.9 million, θ=10°. Both turbulence models use DDES on the NB and OB grids.